International Journal of Solids and Structures 69–70 (2015) 428–441

Contents lists available at ScienceDirect

International Journal of Solids and Structures

journal homepage: www.elsevier.com/locate/ijsolstr

On the compressive failure of tungsten fiber reinforced Zr-based bulk metallic glass composite

J.H. Chen [a], Y. Chen [a,b], M.Q. Jiang [a], X.W. Chen [c], H.F. Zhang [d], L.H. Dai [a,b,*]

[a] State Key Laboratory of Nonlinear Mechanics, Institute of Mechanics, Chinese Academy of Sciences, Beijing 100190, China
[b] State Key Laboratory of Explosion Science and Technology, Beijing Institute of Technology, Beijing 100081, China
[c] Institute of Systems Engineering, China Academy of Engineering Physics, Mianyang, Sichuan 621999, China
[d] Shenyang National Laboratory for Materials Science, Institute of Metal Research, Chinese Academy of Sciences, Shenyang 110016, China

ARTICLE INFO

Article history:
Received 13 August 2014
Received in revised form 4 March 2015
Available online 21 May 2015

Keywords:
Metallic glass
Fiber reinforced composite
Failure mechanism
Shear banding
Splitting
Critical dissipation energy

ABSTRACT

In this paper, a combination of experimentation and analysis is used to identify and study the mechanisms that govern the failure of tungsten fiber reinforced $Zr_{41.2}Ti_{13.8}Cu_{10}Ni_{12.5}Be_{22.5}$ bulk metallic glass composite. In the experimental part, quasi-static and dynamic compressive behaviors of this composite with various fiber volume fractions were systematically investigated. For this composite under uniaxial compression, both the microstructure and strain rate are found to affect the compressive failure behavior. With the increasing fiber volume fraction, or with the decreasing strain rate, the failure mode of the composite switches from shear to splitting. Motivated by the experimental findings, an energy competition mechanism is proposed to unveil these fundamental behaviors of the tungsten fiber reinforced bulk metallic glass composite. The critical energy dissipations for shear banding and splitting of the composite are derived as the functions of tungsten fiber volume fraction and strain rate. It is found that the failure behavior of the composite is decided by the energy competition between shear banding and splitting.

1. Introduction

Bulk metallic glasses (BMGs) are known for their excellent properties including high fracture strength, high hardness, large elastic deflection (Chen, 2008; Lewandowski, 2001; Trexler and Thadhani, 2010; Wang et al., 2009; Gu et al., 2010; Wang, 2012). However, at temperatures well below the glass transition and at high stresses, BMGs undergo inhomogeneous deformation by concentrating severe plastic strain into nanoscale shear bands (Jiang et al., 2008a; Lewandowski and Greer, 2006; Yang et al., 2005; Dai et al., 2005; Greer et al., 2013; Spaepen, 1977; Argon, 1979; Yang et al., 2006; Xu and Ma, 2014). This renders BMGs very limited ductility before catastrophic failure, severely impeding further exploitation of this class of advanced materials. Many investigators have made their efforts to improve the ductility of BMGs (Liu et al., 2007; Yao et al., 2006; Das et al., 2005; Hays et al., 2000; Liu et al., 2005a; Chen et al., 2013). The intrinsic approaches include alloy modification. Lewandowski et al. (2005) proposed the correlation between the intrinsic plasticity or brittleness of the BMGs with the ratio of the elastic shear modulus μ to the bulk modulus B. For metallic glasses alloyed with elements with low μ/B (or, equivalently, high Poisson's ratio) as constituents, the ductility/toughness improves a lot. However, BMGs with high μ/B (or, low Poisson's ratio) exhibit brittle behavior. Gu et al. (2008) also found that the plasticity of BMGs increased with the decrease in shear modulus. Furthermore, they proposed that the plasticity can be significantly improved by chemically tuning the elastic properties which are determined by the amorphous structure and chemical bonding. The extrinsic approaches to improve the plasticity of BMGs are exploring BMG composite. By introducing in situ or ex situ second phases (and/or particles) into the BMG matrix, the BMG composite has yielded improvements in tensile and compressive strains to failure (Hays et al., 2000; Qiao et al., 2011; Yim et al., 1999; Hofmann et al., 2008a; Martin et al., 2009; Wu et al., 2011; Chen et al., 2013; Hofmann et al., 2008b). For instance, the in situ Zr-based BMG composite shows the tensile fracture strain as high as 10% (Wu et al., 2010; Hofmann et al., 2008a). The increase in ductility has been attributed to that the second phase can restrict the propagation of shear band, and on the other hand, promote the generation of multiple shear bands. These multiple shear bands can accommodate much plastic strain, which contributes to macroscopic plasticity.

* Corresponding author at: State Key Laboratory of Nonlinear Mechanics, Institute of Mechanics, Chinese Academy of Sciences, Beijing 100190, China. Tel.: +86 10 82543958; fax: +86 10 82543977.
E-mail address: lhdai@lnm.imech.ac.cn (L.H. Dai).

http://dx.doi.org/10.1016/j.ijsolstr.2015.05.008
0020-7683/

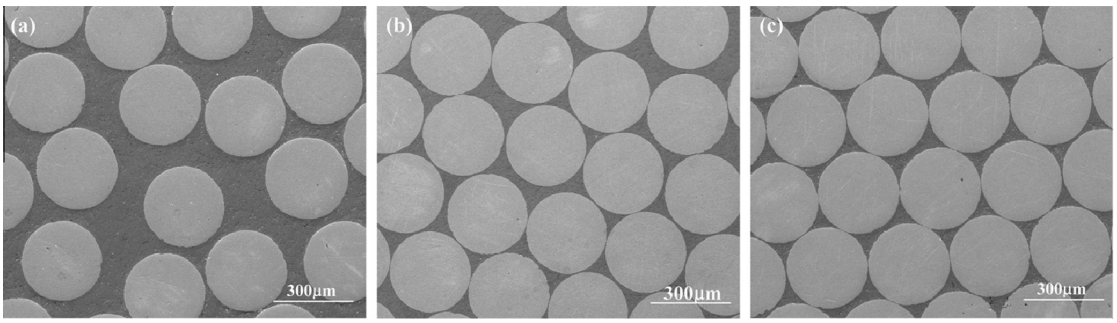

Fig. 1. Microstructures of the tungsten fiber/Vit 1 BMG composite with different fiber volume fractions. (a) 40% V_f. (b) 60% V_f. (c) 80% V_f.

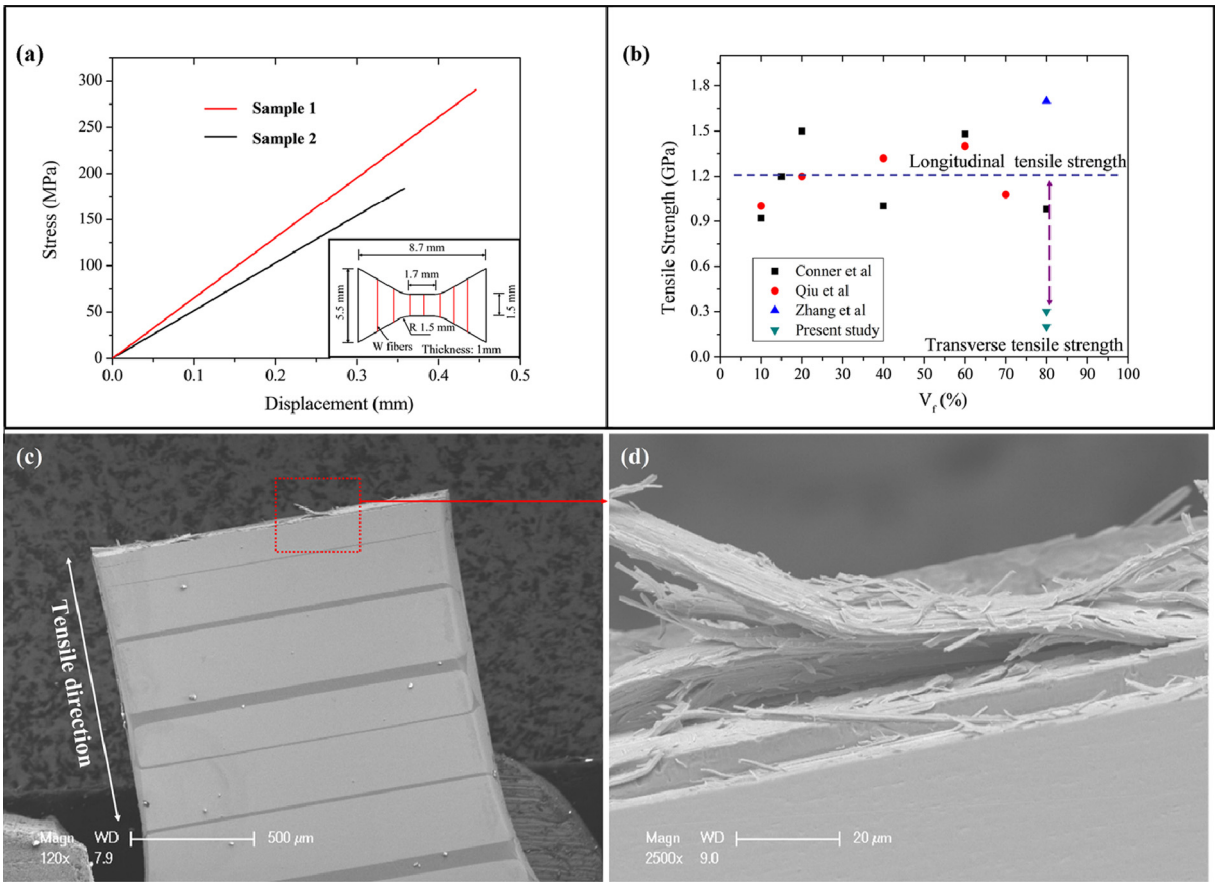

Fig. 2. (a) Transverse tensile stress-displacement curve of the composite with 80% V_f. The insert shows the dimensions of the tested specimen. (b) Comparison of the transverse tensile strength with the longitudinal tensile strength obtained from previous studies. (c) Specimen of the composite after fracture. (d) Magnified image corresponding to the marked areas in (c).

The tungsten fiber reinforced BMG composite was first fabricated by Dandliker et al. (1998). This composite demonstrates considerable plasticity under both quasi-static and dynamic compression (Conner et al., 1998; Qiu et al., 2002; Wang et al., 2006; Hou et al., 2007; Wang et al., 2007; Zhang et al., 2009). Furthermore, under high speed impact, this composite exhibits "self-sharpening" behavior, resulting in a 10–20% improvement in penetrator efficiency over the traditional tungsten heavy alloy (Conner et al., 2000). This promotes the tungsten fiber reinforced BMG composite to be used in the defense field. In the past few years, many studies have been carried out on the macroscopic properties of this composite. Conner et al. (1998) performed quasi-static compressive experiments on the tungsten fiber reinforced $Zr_{41.2}Ti_{13.8}Cu_{12.5}Ni_{10}Be_{22.5}$ BMG composite with various fiber volume fractions. It was found by them that the compressive failure mode of this composite changes from the shear banding to fiber buckling as fiber volume fraction increases. The mechanical properties of tungsten fiber reinforced ZrAlNiCuSi BMG composite under quasi-static compression was investigated by Qiu et al. (2002). Their experimental results are consistent with the observations of Conner et al. (1998). Lee et al. (2008) tested the mechanical properties of the tungsten and STS 304 stainless steel continuous fiber reinforced BMG composite. Though these two composites have the similar fiber volume fraction, their failure behaviors are totally different. The tungsten fiber/BMG composite has a higher strength but a lower plasticity, while the STS 304 stainless steel continuous fiber/BMG composite exhibits a lower strength but higher plasticity. Through the compressive tests of tungsten fiber

reinforced BMG composite, Zhang et al. (2008) reported that the shear band patterns in the matrix are different for different fiber separations. For the matrix with low lateral confinement, the shear bands are in plane. However, shear bands propagate out-of-plane in the matrix with high lateral confinement. It can be seen that the compressive properties of the tungsten fiber reinforced BMG matrix composite are strongly affected by the microstructure.

For BMG alone, it was proposed by Sunny et al. (2007, 2008, 2009) and Yuan et al. (2007, 2009) that this material is insensitive to the strain rate. However, besides the microstructure, strain rate is also found to have noticeable influence on the compressive properties of the tungsten fiber reinforced BMG matrix composite. Conner et al. (2000) conducted quasi-static and dynamic compressive experiments on the tungsten fiber reinforced $Zr_{41.2}Ti_{13.8}Cu_{12.5}Ni_{10}Be_{22.5}$ BMG composite. They found that for the composite with 60% fiber volume fraction, the failure mode is fiber splitting, buckling and localized tilting in the quasi-static case, while at dynamic compression, this composite fails by localized shear banding. They pointed out that the shear becomes the preferred failure mechanism as strain rate increases, even in samples with a large volume fraction of reinforcement. These are confirmed by the experimental observations of Ma et al. (2008).

The above mentioned investigations suggest that both the microstructure and strain rate affect the compressive failure behavior of the tungsten fiber reinforced BMG composite. However, a number of important questions arise from these observations. What is the controlling factor for the transition of failure mode of the composite? How to quantitatively describe the influence of the microstructure and strain rate on the compressive failure behavior of this composite? From the experimental observations, two major micro-damages are observed for this composite. One is shear banding, the other is splitting (Conner et al., 1998; Qiu et al., 2002; Zhang et al., 2009). It was proposed by Grady (1992), Grady (1994), Jiang and Dai (2011) that the resistance of materials to shear band propagation can be measured by the critical plastic energy dissipated in the shear band, which is affected by the strain rate. The composite contains both the crystalline tungsten fiber and amorphous matrix. These two phases have different intrinsic microstructures and energy dissipation mechanism of shear banding (Grady, 1992; Grady, 1994; Jiang and Dai, 2011; Dai, 2012). Thus, the critical dissipation energy in the shear band of tungsten fiber/BMG composite should depend on the relative volume ratio of its component phases and strain rate. Furthermore, it was proposed by Zhang et al. (2006) that the longitudinal splitting fracture of the composite may be caused by the transverse tensile strain. From the aspect of energy, it can be speculated that when the deformation energy stored in the composite overcomes the critical deformation energy, longitudinal splitting fracture may occur. Thus, the critical deformation energy stored in the composite, which is influenced by the tungsten fiber volume fraction and strain rate, can also measure the resistance to splitting fracture of the composite. The compressive failure behavior of the composite may be decided by the competition between the critical energy dissipated in the shear band and the critical deformation energy stored in the composite, which deserved further investigations.

In this study, transverse tensile, quasi-static and dynamic compressive tests were systematically conducted on the tungsten fiber reinforced $Zr_{41.2}Ti_{13.8}Cu_{10}Ni_{12.5}Be_{22.5}$ BMG composites with 0%, 40%, 60% and 80% tungsten fiber volume fraction. For each tested specimen, the shear banding and fracture behavior are carefully examined by the high-resolution scanning electron microscopy (SEM) and the high speed camera. Based on the experimental observations, an energy competition mechanism is developed to unveil the compressive failure behavior of the composite. The critical energy dissipated in the shear band and the critical deformation energy stored in the composite as the functions of fiber volume fraction and strain rate are obtained. Our results should assist in comprehensively understanding compressive failure mechanism, and in guiding microstructure design to enhance the plasticity of bulk metallic glass composite.

2. Experiments

The chemical composition of the matrix is $Zr_{41.2}Ti_{13.8}Cu_{10}Ni_{12.5}Be_{22.5}$ (Vit 1). This BMG is obtained by arc-melting the elements Zr, Ti, Cu, Ni and Be (with a purity of 99.9% or better) together in a Ti-getterred high-purity argon atmosphere. As-drawn tungsten fiber, with the nominal diameter of 300 μm, is used as the reinforcement. Tungsten fiber/BMG matrix composite is prepared using infiltration and rapid solidification method. Details of the casting can be found elsewhere (Dandliker et al., 1998). Microstructures of the composite with 40%, 60% and 80% tungsten fiber volume fraction are shown in Fig. 1(a)–(c), respectively.

All the tested specimens are obtained by wire electrical discharge machining the as-cast composite rods using coolant. According to the previous study (Zhang et al., 2006), the longitudinal splitting fracture of the composite during compression may relate to the transverse tensile properties. In order to obtain the transverse tensile properties of the composite, in situ tensile tests were conducted on the composite with 80% fiber volume fraction using a FEI Sirion scanning electron microscope (SEM). Dimensions of the specimen for in situ tension measurement are shown in the insert of Fig. 2(a). The surfaces of the specimen were mechanically polished to mirror finish. The fibers in the specimen

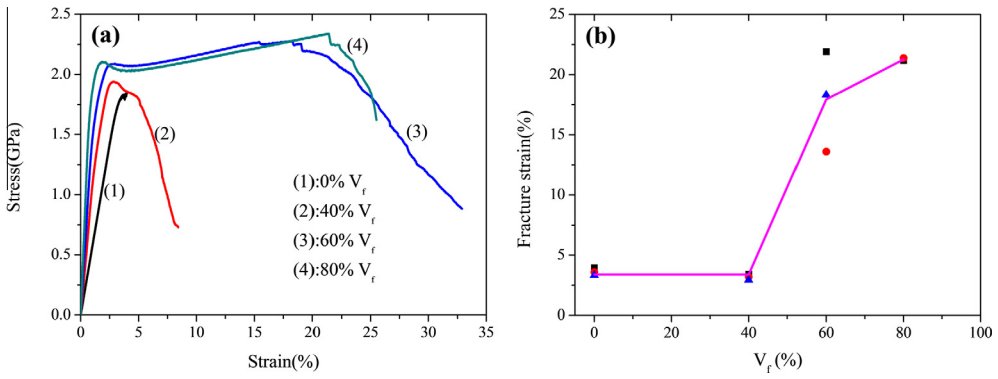

Fig. 3. (a) Stress–strain curves of the composite with different fiber volume fractions under quasi-static compression. (b) Fracture strain of the composite varies with the fiber volume fraction V_f under quasi-static compression.

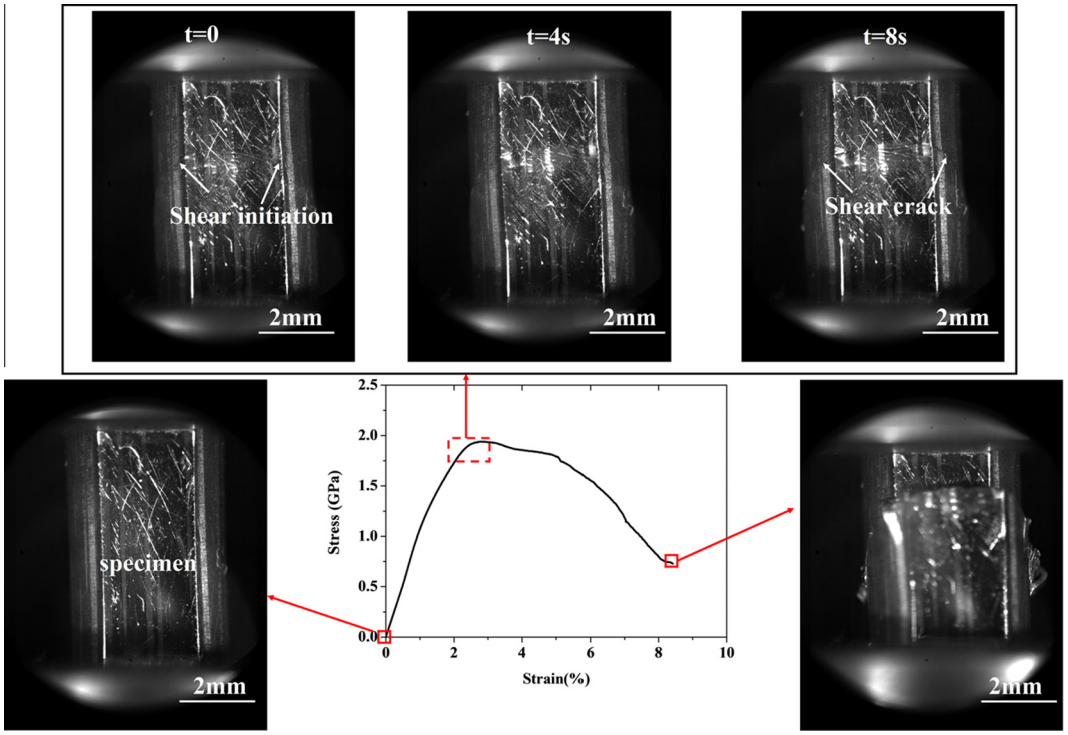

Fig. 4. Deformation process of the composite with 40% V_f under quasi-static compression. Imitation and propagation of the shear deformation are also captured by the high speed camera.

are unidirectionally aligned in the direction perpendicular to the tensile direction. Quasi-static and dynamic compressive tests were conducted on the composites with 0% (Vit 1), 40%, 60% and 80% fiber volume fraction, respectively. Specimens for compression tests have the same dimensions, which are 5 mm in diameter and 8 mm in length. The specimen end surfaces are polished to be parallel to each other and perpendicular to the loading axis. Quasi-static and dynamic compressive tests were performed on an MTS-810 material machine and a split Hopkinsion pressure bar (SHPB), respectively. In quasi-static compressive tests, the average strain rate, estimated by the velocity of the load head and sample length, was about 7.0×10^{-4}/s. In the SHPB dynamic compressive experiments, the average strain rate is about 2.0×10^{3}/s by controlling impact velocity. To better understand the deformation process of the composite, a high speed camera, with a maximum framing rate capability of 300 thousand frames per second is used to capture the quasi-static deformation process. After testing, the SEM is used to characterize the microscopic deformation of all specimens.

3. Results

3.1. Transverse tensile tests

Fig. 2(a) shows the results of the transverse tensile tests of the composite with 80% fiber volume fraction (V_f). No plastic deformation can be observed before fracture. The transverse tensile strength of the composite is only about 200–300 MPa. Comparison of the transverse strength with longitudinal tensile strength, which is obtained from the previous studies, is shown in Fig. 2(b). It can be seen that the transverse strength is one order of magnitude lower than the longitudinal strength. Transverse tensile fracture morphologies are shown in Fig. 2(c) and (d). Layered fibers are pulled out from the fracture surface, as shown in Fig. 2(d).

It can be seen from the transverse tensile tests that the tungsten fiber/BMG matrix composite is not an isotropic material. Actually, the as-drawn tungsten fiber has fibrous grain structure along the axial direction (Zhang et al., 2006; Son et al., 2012). It has been estimated that the lateral grain boundary strength of a tungsten fiber with fibrous grain structure is only about 14% of its axial tensile strength (Varge et al., 1974). Therefore, the axial properties of the tungsten fiber are totally different from its lateral properties. From this aspect, the tungsten fiber/BMG matrix composite can be regarded as a transversely isotropic material.

3.2. Quasi-static compressive tests

Fig. 3(a) shows the typical stress–strain curves of the composite with 0% (Vit1 BMG), 40%, 60% and 80% V_f under a quasi-static strain rate of 7.0×10^{-4}/s. It can be seen that the 0% (Vit1 BMG) and 40% V_f composites fracture in a brittle manner with limited plasticity. However, 60% and 80% V_f composites exhibit the plastic strain as high as 20% before failure. The fracture strain of the composite varied with V_f is shown in Fig. 3(b). With the increasing V_f, the plasticity of the composite increases. Detailed discussions of each kind of composite are shown in the following paragraphs.

Fig. 4 shows the deformation process of the 40% V_f composite imaged by the high speed camera. It can be seen clearly that shear fracture occurs in this composite at the end of deformation. The evolution of shear deformation is also captured by the high speed camera. At $t = 0$, shear band initiate at the specimen surface. At about $t = 8$ s, the shear band evolves into the shear crack. Simultaneously, the stress begins to drop and the composite begins to lose its load capacity. From this figure, it can be concluded that the critical time for shear band to propagate in the composite is on the order of 10^0 s.

The fracture morphologies of the 40% V_f composite are shown in Fig. 5. Fig. 5(b) shows details corresponding to the area marked in Fig. 5(a). It can be seen that shear banding in the BMG matrix

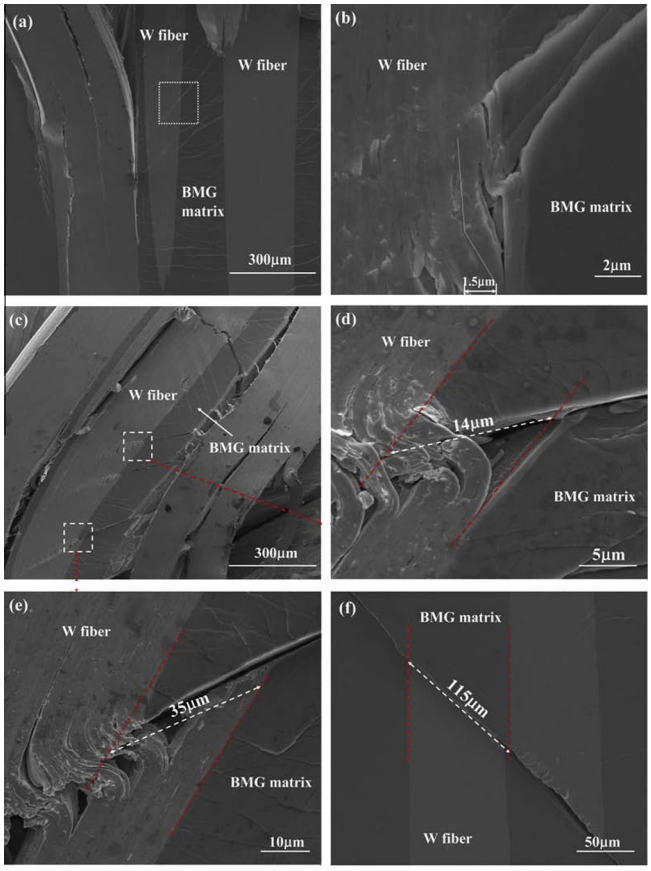

Fig. 5. Fracture morphologies of the 40% V_f under quasi-static compression. (a) Lateral surface of the fractured specimen. (b) Magnified image of the area marked in (a). (c) Another region on the lateral surface of the fractured specimen. (d) And (e) Details corresponding to the areas marked in (c). (f) Another area on the lateral surface, showing the shear fracture of the tungsten fiber.

induces shear deformation in the tungsten fiber. The shear displacement within shear band in tungsten fiber is about 1.5 μm. Fig. 5(d) and (e) are magnified SEM pictures corresponding to the areas marked in Fig. 5(c). At the larger shear displacement, i.e., 14 μm in Fig. 5(d) and 35 μm in Fig. 5(e), shear bands in the BMG matrix evolve into shear cracks. These shear cracks induce more severe shear deformation in the tungsten fiber. However, shear cracking do not take place in the tungsten fiber. Fig. 5(f) shows the shear banding in another place of the specimen. Under the shear displacement of 115 μm, the shear crack crosses through both the BMG matrix and tungsten fiber. It can be estimated from Fig. 5 that the critical shear displacement of the tungsten fiber is about 10^1 μm. Fig. 6 shows details within the shear band in the tungsten fiber. Under the shear displacement of 30 μm, shear cracking in the BMG matrix induces shear banding in the tungsten fiber. Fibrous structure is observed within the shear band of tungsten fiber, as shown in Fig. 6(c). This is due to the intrinsic fibrous microstructure of the as drawn tungsten fiber. Furthermore, it can be seen from this figure that the width of the shear band in tungsten fiber is about 10 μm. Thus, it can be obtained from Fig. 5 and Fig. 6 that the critical shear strain of the tungsten fiber can be estimated as $\gamma = 10^1\ \mu m/10^1\ \mu m \approx 10^0$. Because of the critical time of shear band evolution is 10^0 s, the local shear strain rate of the tungsten fiber in 40% V_f composite is on the order of 10^0/s.

Deformation process of the 60% V_f composite is shown in Fig. 7. At the strain of 14.8%, splitting occurs in the middle of the specimen, as can be seen from Fig. 7(d). Upon further loading, the splitting crack propagates towards two ends of the specimen. At 23.4% strain, the composite begins to soften and loses its load capacity. The 60% V_f composite fractures in the splitting dominated mode. Fig. 8 shows the fracture morphologies of the 60% V_f composite. From Fig. 8(a), it can be seen that besides splitting fracture, shear fracture also occurs in the local region of the specimen. Fig. 8(b), (c) and (e) are magnified images corresponding to the areas (1)-(3) marked in Fig. 8(a), respectively. Numerous shear bands can be observed in the BMG matrix, as shown by the arrows in Fig. 8(c) and (e). However, these shear bands are restrained in

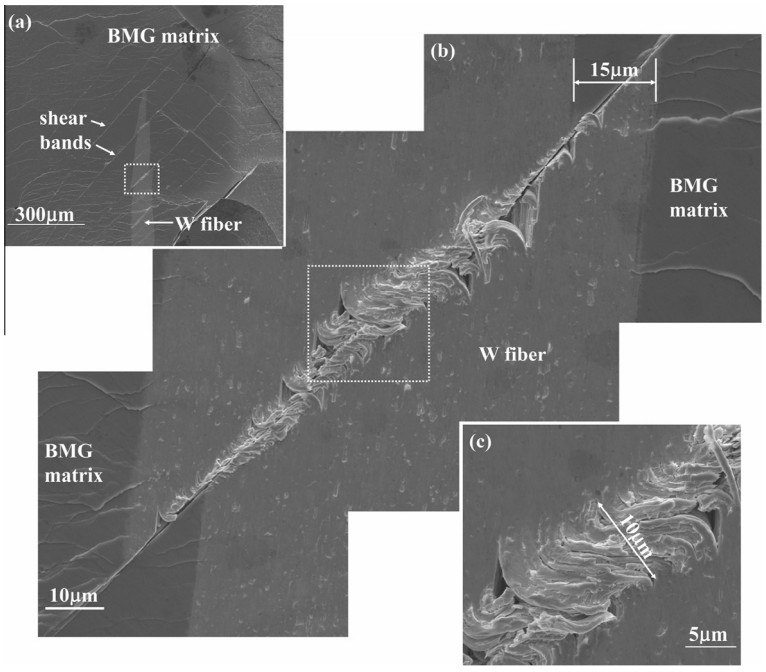

Fig. 6. Details of the shear banding in tungsten fiber. (a) Lateral surface of the specimen of composite with 40% V_f under quasi-static compression. (b) Details corresponding to the area marked in (a), showing the shear banding of the tungsten fiber. (c) Magnified image of the marked area in (b), giving the details within shear band of tungsten fiber.

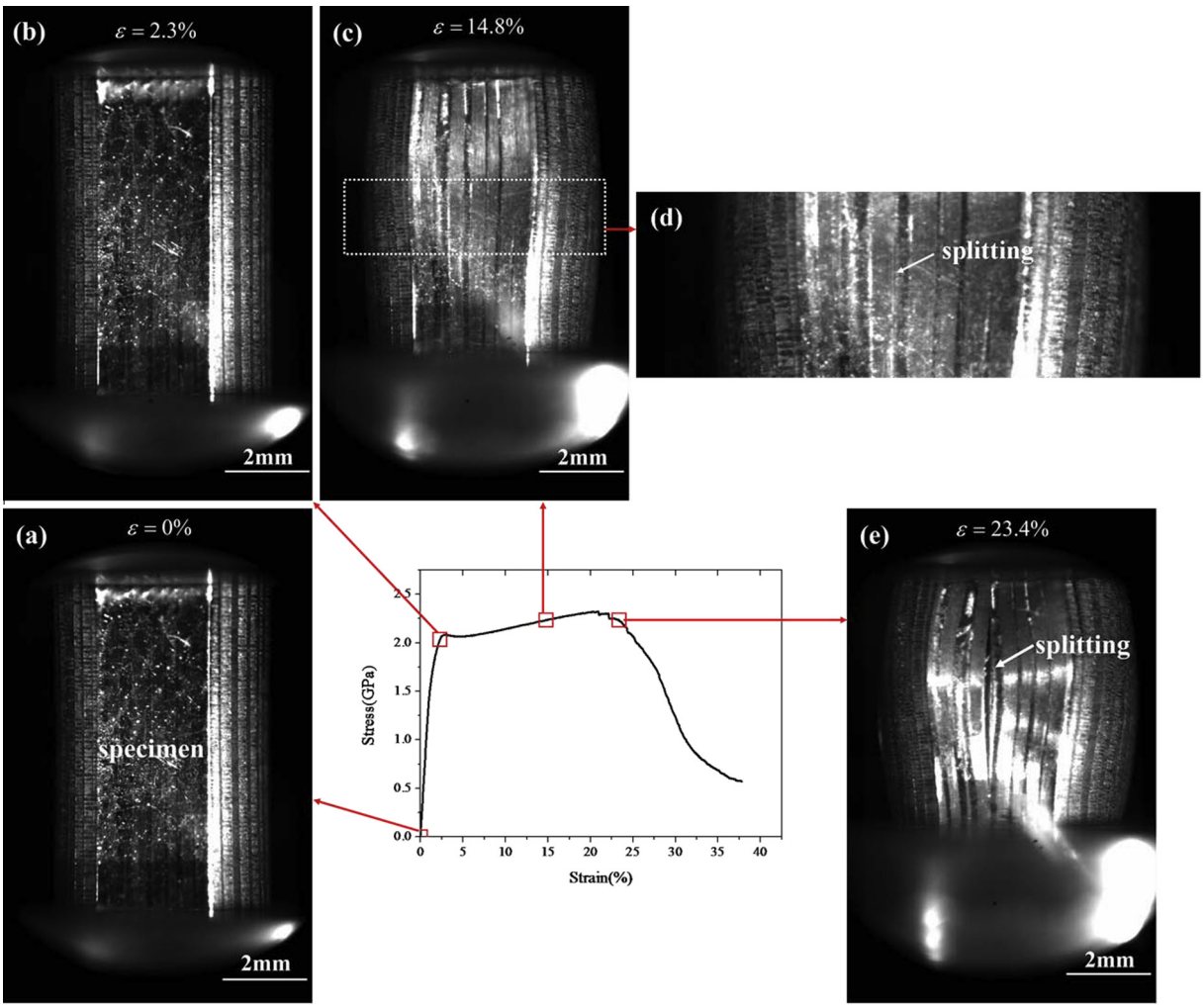

Fig. 7. Deformation process of the 60% V_f composite imaged by the high speed camera under quasi-static compression. (a) Specimen of the composite at the beginning of deformation. (b) Specimen of the composite at the beginning of yielding. (c) Splitting occurs for the composite. (d) Magnified image of the area marked in (c). (e) Softening occurs for the specimen and the composite begins to lose its load capacity.

the matrix and cannot cross through the tungsten fiber, as shown in Fig. 8(d) and (f), which show the details corresponding to the marked areas in Fig. 8(c) and (e), respectively. This shear band pattern is totally different from that observed in the 40% V_f composite.

Fig. 9 shows the deformation process of the 80% V_f composite. At a small strain of 5.2%, the splitting occurs in the specimen, as shown in Fig. 9(d). Finally, the composite fails in the splitting mode. The fracture morphologies of the 80% V_f composite are shown in Fig. 10. Only splitting fracture can be observed, no shear fracture occurs. Fig. 10(b) shows the details of splitting crack. Fibrous structure, which is similar to the pattern of the tungsten fiber under transverse tension, can be observed. According to the previous studies (Zhang et al., 2006; Son et al., 2012), the as-drawn tungsten fiber has extreme texture. It has fibrous grain structure along the axial direction. It can be seen from the transverse tensile tests that the lateral tensile strength of a tungsten fiber with fibrous grain structure is much lower than its axial tensile strength. Longitudinal compression will create lateral tensile strain, which results in the propagation of splitting in the composite. Actually, from Fig. 10(b), it can be seen that the splitting fracture always happens within the tungsten fiber. In our other work (Chen et al., 2014), the deformation process of this composite is investigated carefully. It was found that the splitting initiate within the tungsten fiber near the fiber/matrix interface region. Fig. 10(c) and (e) are magnified images corresponding to the areas (1) and (2) marked in Fig. 10(a), respectively. Similar to the shear band pattern observed in the 60% V_f composite, the shear bands are hindered by the tungsten fiber, as shown in Fig. 10(d) and (f).

From the quasi-static compressive tests, it can be seen that with the increasing V_f, failure mode of the tungsten fiber/BMG matrix composite changes from shear to splitting. Critical stress and strain of the tungsten fiber/BMG matrix composite under quasi-static compression are summarized in Table 1. The critical stresses for splitting of 60% and 80% V_f composite are about the same. However, the critical strain for splitting of the 60% V_f composite is higher than that of the 80% V_f composite, indicating splitting fracture becomes easy with the increasing V_f.

3.3. Dynamic compressive tests

Dynamic stress–strain curves of the tungsten fiber/BMG composite with 0%, 40%, 60% and 80% V_f are shown in Fig. 11(a). Similar to the quasi-static condition, under dynamic compression, composite with 0% and 40% V_f fail with limited plasticity, while the 60% and 80% V_f composite exhibit large plasticity. With the increasing V_f, the fracture strain of the tungsten fiber/BMG composite increases, as shown in Fig. 11(b).

Under the dynamic strain rate, the 40% V_f composite fractures into many pieces. Since the failure mode can be distinguished by the fracture morphologies, these pieces are carefully examined

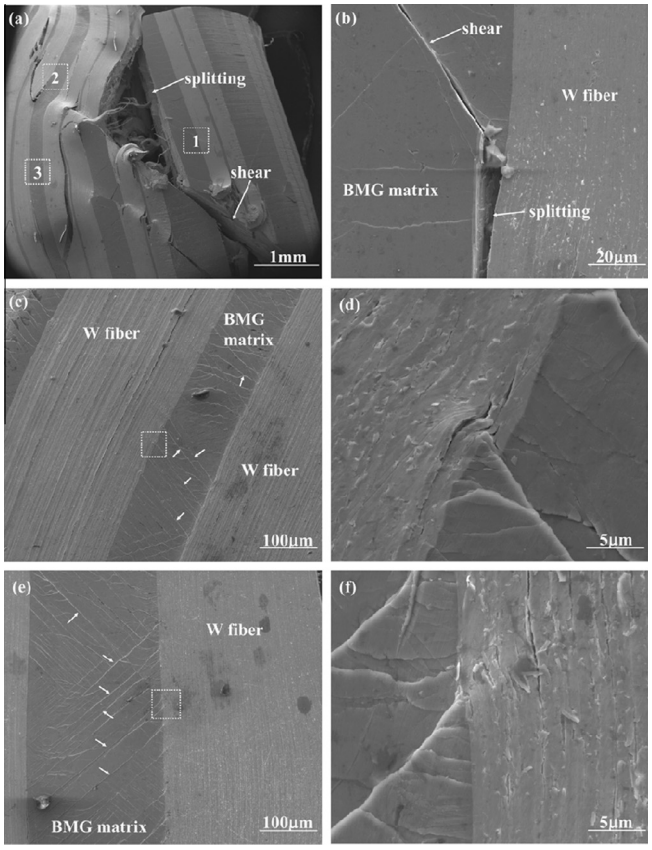

Fig. 8. Fracture morphologies of the 60% V_f under quasi-static compression. (a) Lateral surface of fractured specimen. (b), (c) and (e) are magnified images of the areas marked by (1)-(3) in (a), respectively. Multiple shear bands in the BMG matrix are indicated by the arrows. (d) And (f) show details corresponding to the marked area in (c) and (e), respectively.

by the SEM. The fracture morphologies of one of these pieces are shown in Fig. 12. Cell-like vein pattern, which is the typical shear fracture morphology (Liu et al., 2005b; Jiang et al., 2008b; Martin et al., 2008), can be observed on the BMG matrix, as shown in Fig. 12(c). It can be seen from Fig. 12(d) that the tungsten fiber exhibits a stair-step-like pattern. According to the study by Leber et al. (1976), this is the typical shear morphology of tungsten fiber. It can be concluded from these that the 40% V_f composite fractures by shear.

Fig. 13 shows the fracture morphologies of the 60% V_f composite. Shear becomes the dominant failure mode of this composite. This result is consistent with the observation of Conner et al. Fig. 13(b), (c) and (e) are details corresponding to the areas marked by (1)-(3) in Fig. 13(a), respectively. Both in-plane and out-plane shearing occur for this composite, as can be seen in Fig. 13(b). Multiple shear bands can be observed in the BMG matrix, as indicated by the arrows in Fig. 13(c) and (e). In some local regions, shear bands are hindered by the tungsten fiber (Fig. 13(d)). However, shear banding in the matrix can induce shear deformation in the tungsten fiber in other local region, as shown in Fig. 13(f). This is different from that observed under quasi-static compression.

Fig. 14 gives the fracture morphologies of the 80% V_f composite. Fig. 14(a) is the lateral morphologies imaged by the optical microscope. It can be seen clearly that the composite fails by splitting fracture. Fig. 14(c) and (e) are magnified images of the areas marked in Fig. 14(b) and (d), respectively. Shear bands in the matrix are indicated by the arrows. Similar to the quasi-static condition, shear bands are constrained in the BMG matrix.

3.4. Information extracted from experiments

The experimental results and observations reveal some crucial features of tungsten fiber/BMG composite behavior during failure, as follows:

(1) Transverse tensile strength is one order lower than longitudinal tensile strength, indicating the tungsten fiber/BMG composite is a transversely isotropic material. This low transverse tensile strength will lead to longitudinal splitting of the composite under compression.
(2) The compressive failure behavior of the composite is affected by both the fiber volume fraction V_f and strain rate. Under both the quasi-static and dynamic strain rate, with the increasing V_f, failure mode of the composite changes from shear to splitting. Furthermore, for 60% V_f composite, with the strain rate increases from quasi-static to dynamic, splitting dominated fracture shifts to shearing dominated fracture. This demonstrates that the critical fiber volume fraction V_c, corresponding to the transition from shear to split fracture, increases with the increasing strain rate. Shearing is more likely to happen at high strain rate.
(3) Two kinds of micro-damage, shear banding and splitting, are observed under both quasi-static and dynamic compression of the composite. For composite with low V_f, shear banding in the BMG matrix can induce shear deformation in the tungsten fiber. However, shear banding is hindered by the tungsten fiber for composite with large V_f. This reveals that shear fracture of the composite becomes difficult with the increasing V_f. Furthermore, critical strain for splitting of the 80% V_f composite is lower than that of the 60% V_f composite, indicating splitting fracture becomes easy with the increasing V_f. It can be concluded that the failure mode of the composite may be determined by the competition between the shear banding and splitting, which will be discussed in the next sections.

4. Energy competition mechanism

In this section, an energy competition mechanism is proposed to characterize the compressive failure behavior of the composite.

It is well known that the shear banding process is a dissipation system (Zhang et al., 2008; Dai and Bai, 2008; Conner et al., 2004; Jiang and Dai, 2009; Meyers et al., 2001; Yang et al., 2010; Ruan et al., 2011). It will dissipate energy within shear band during its propagation. Once the energy release overcomes the critical energy dissipated in a shear band, the shear band will mature as a runway shear crack. The critical energy dissipated in the shear band therefore determines the shear band susceptibility, which measures the intrinsic resistance of materials to the propagation of shear bands. In addition, longitudinal compression will create lateral tensile strain. Once the lateral tensile strain overcomes the critical lateral tensile strain of the composite, longitudinal splitting will occur. From the aspect of energy, once the deformation energy overcomes the critical deformation energy stored in the composite, longitudinal splitting will occur. Thus, the critical deformation energy for splitting can also measure the resistance of composite to splitting fracture. Essentially, the competition between shear banding and splitting can be discussed from the viewpoints of energy dissipation. For simplicity, in our analysis, it assumes that the composite behaves elastically when calculating the critical energy.

4.1. Critical shear band dissipation energy

In Grady's (1992, 1994) work, thermal and momentum dissipation are considered within the shear band of crystalline alloy. The

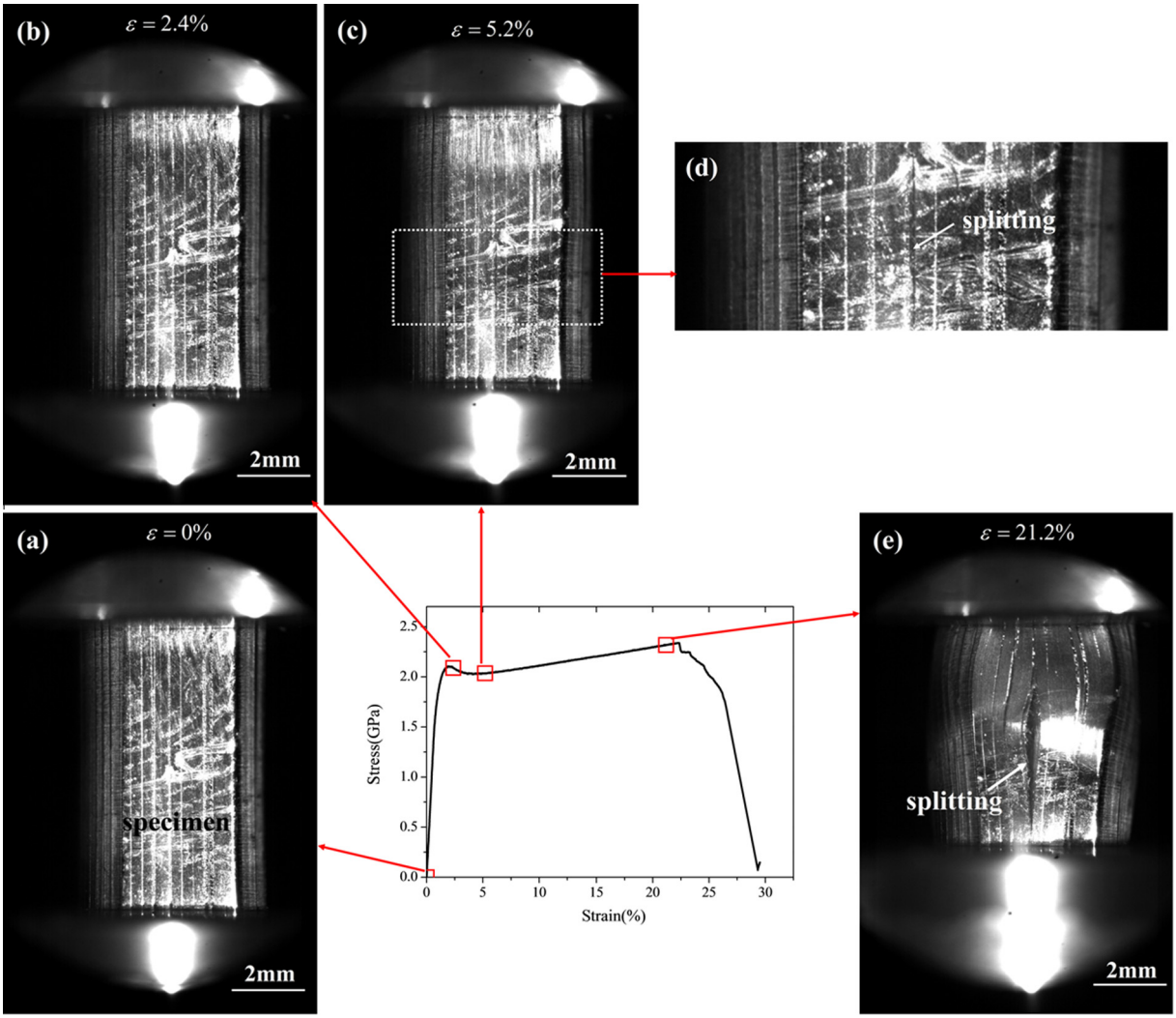

Fig. 9. Deformation process of the 80% V_f composite imaged by the high speed camera under quasi-static compression. (a) At the beginning of deformation. (b) Yielding of the composite. (c) Splitting begins of the specimen. (d) Magnified image of the area marked in (c). (e) Final failure of the composite.

critical energy dissipated per unit area within shear band can be given by:

$$\Gamma_f = \frac{\rho c}{\alpha}\left(\frac{9\rho^3 c^2 \chi^3}{\tau_y^3 \alpha^2 \dot{\gamma}}\right)^{1/4} \tag{1}$$

where ρ is the density of the material, α is the thermal softening coefficient, c and χ are bulk specific heat and thermal diffusivity coefficients, respectively, $\dot{\gamma}$ is the shear strain rate and τ_y is the yield strength.

In our previous work (Jiang and Dai, 2011), the concept of critical dissipation energy within shear band was developed in the BMGs. In addition to conventional thermal and momentum dissipation, the free volume dissipation should be involved due to the unique atomic structure of BMGs. Actually, Jiang and Dai (2011) have pointed out that the thermal effect plays a secondary role in the critical dissipation energy within shear band in BMGs. Considering the shear band stress softening only due to free volume creation, the explicit expression of critical energy dissipated per unit area within shear band can be expressed by

$$\Gamma_m = \frac{\tau_y}{\beta R}\left(\frac{9\rho D^3}{\dot{\gamma}\tau_y \beta^2 R^2}\right)^{1/4} \tag{2}$$

where β is free volume softening coefficient, D is the diffusion coefficient of free volume concentration, R describes the local dilatation ability.

Tungsten fiber/BMG composite contains both the crystalline tungsten fiber and amorphous matrix. Critical energy dissipated per unit area within shear band of the composite can be obtained from the tungsten fiber and BMG matrix by the rule of mixture:

$$\Gamma_{SB} = \Gamma_m(1 - V_f) + \Gamma_f V_f \tag{3}$$

It can be seen from Eqs. (1)-(3) that critical dissipation energy within shear band of the composite is the function of fiber volume fraction V_f and strain rate $\dot{\gamma}$. Substituting the parameters of tungsten fiber and Vit 1 BMG into Eqs. (1)-(3), the critical dissipation energy within shear band of tungsten fiber/Vit 1 BMG composite can be obtained at the specific V_f and strain rate $\dot{\gamma}$.

4.2. Critical energy for splitting

It can be seen from the transverse tensile tests that the tungsten fiber/Vit 1 BMG composite has weak transverse tensile strength, which leads to low transverse critical tensile strain. Once the lateral strain created by the longitudinal compression overcomes the transverse critical tensile strain, splitting fracture occurs. It

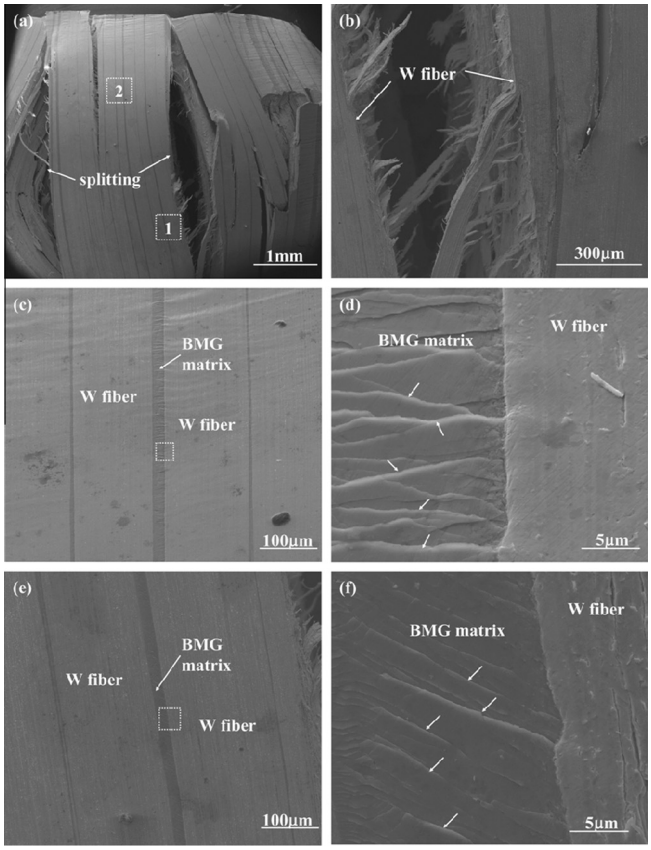

Fig. 10. Fracture morphologies of the 80% V_f under quasi-static compression. (a) Lateral surface of fractured specimen. (b) Details of the splitting crack of the composite. (c) And (e) are magnified images of the areas marked by (1) and (2) in (a), respectively. (d) And (f) show details corresponding to the areas marked in (c) and (e), respectively. Multiple shear bands are shown by the arrows.

can be also obtained from the experimental results that the tungsten fiber/Vit 1 BMG composite can be treated as a transversely isotropic material. For simplification, the longitudinal direction of the composite, which is parallel to the fiber direction, is marked as "1", while the transverse (lateral) direction of the composite, which is perpendicular to the fiber direction, is marked as "2". The critical deformation energy for splitting will be calculated in the following paragraphs.

The transverse tensile strength of the tungsten fiber/Vit 1 BMG composite can be obtained by the rule of mixture:

$$\sigma_2 = \sigma_m(1 - V_f) + \sigma_f V_f \tag{4}$$

Here, σ_m and σ_f are the transverse tensile strength of the Vit 1 BMG and tungsten fiber, respectively, which are considered to be independent on the strain rate. Actually, many previous studies exhibit that the strength of BMG is insensitive to the strain rate, or the strength of BMG decreases with the increasing strain rate with a small strain rate sensitivity (Bruck et al., 1996; Subhash et al., 2002; Li et al., 2003; Sunny et al., 2007, 2008, 2009; Yuan et al., 2007, 2009). Thus, it is reasonable to propose that the transverse strength of the composite is insensitive to the strain rate. The transverse elastic modulus of the transversely isotropic composite can be given by

$$E_2 = \frac{E_m E_f}{E_m V_f + E_f(1 - V_f)} \tag{5}$$

$E_m$and E_f are the elastic modulus of the Vit 1 BMG and tungsten fiber, respectively. Thus, the transverse critical tensile strain can be obtained from transverse tensile strength σ_2 and elastic modulus E_2, expressed as

$$\varepsilon_2 = \frac{[\sigma_m(1 - V_f) + \sigma_f V_f]\,[E_m V_f + E_f(1 - V_f)]}{E_m E_f} \tag{6}$$

The longitudinal compressive critical strain ε_1 can be related to the transverse tensile critical strain ε_2 by the Poisson's ratio ν_{12}, which is given by

$$\nu_{12} = \nu_m(1 - V_f) + \nu_f V_f \tag{7}$$

ν_m and ν_f are the Poisson's ratio of the Vit 1 BMG and tungsten fiber, respectively. Then, ε_1 is obtained,

$$\varepsilon_1 = \frac{[\sigma_m(1 - V_f) + \sigma_f V_f]\,[E_m V_f + E_f(1 - V_f)]}{E_m E_f[\nu_m(1 - V_f) + \nu_f V_f]} \tag{8}$$

We now introduce the critical energy Γ_{SP} stored in the composite as deformation proceeds to a critical strain ε_1. Similar to the concept of critical energy dissipated per unit area within shear band, Γ_{SP} is the deformation energy per unit area within the cross section of the specimen, identified as

$$\Gamma_{SP} = \frac{1}{2}\sigma_1 \Delta l = \frac{1}{2}E_1 \varepsilon_1^2 l \tag{9}$$

l is the length of the tested specimen. E_1 is the longitudinal elastic modulus of the composite, as given by

$$E_1 = E_m(1 - V_f) + E_f V_f \tag{10}$$

Eqs. (8)-(10) give the analytical expression of the critical energy Γ_{SP} for splitting. In this study, Γ_{SP} is only the function of the fiber volume fraction V_f. This is due to that the transverse strength of the composite is considered to be insensitive to the strain rate, as shown in Eq. (4). The critical energy Γ_{SP} at a given V_f can be obtained by substituting the parameters of the Vit 1 BMG and tungsten fiber into Eqs. (8)-(10).

4.3. Competition between the two critical energies

The thermodynamic parameters of tungsten fiber are given in Table 2. Using these parameters and Eq. (1), the critical energy dissipated within the shear band of crystalline tungsten fiber Γ_f can be calculated. In our previous work (Jiang and Dai, 2011), based on Eq. (2), the critical energy dissipated within the shear band of Vit1 BMG Γ_m is obtained. Substituting Γ_m and Γ_f into Eq. (3), we obtain that the critical energy dissipated within the shear band of tungsten fiber/Vit 1 composite Γ_{SB} varies with the fiber volume fraction V_f under different strain rates, as shown in Fig. 15. Strength, Poisson's ratio and elastic modulus of the tungsten fiber and Vit 1 BMG are shown in Table 3 (Conner et al., 1998). Substituting these parameters into Eqs. (8)-(10), the critical energy for splitting of the tungsten fiber/Vit 1 composite Γ_{SP} as a function of fiber volume fraction V_f can also be obtained, which is shown in Fig. 15.

It can be seen from Fig. 15 that under a specific strain rate, the critical energy dissipated within the shear band of tungsten fiber/Vit 1 composite Γ_{SB} increases with the increasing fiber volume fraction V_f. This indicates that the resistance to the shear band

Table 1
Critical stress and strain of the composite for shear and splitting under quasi-static compression.

	40% V_f	60% V_f	80% V_f
Critical shear strain	3.2%	–	–
Critical shear stress (GPa)	1.9	–	–
Critical strain for splitting	–	14.9%	5.2%
Critical stress for splitting (GPa)	–	2.2	2.0

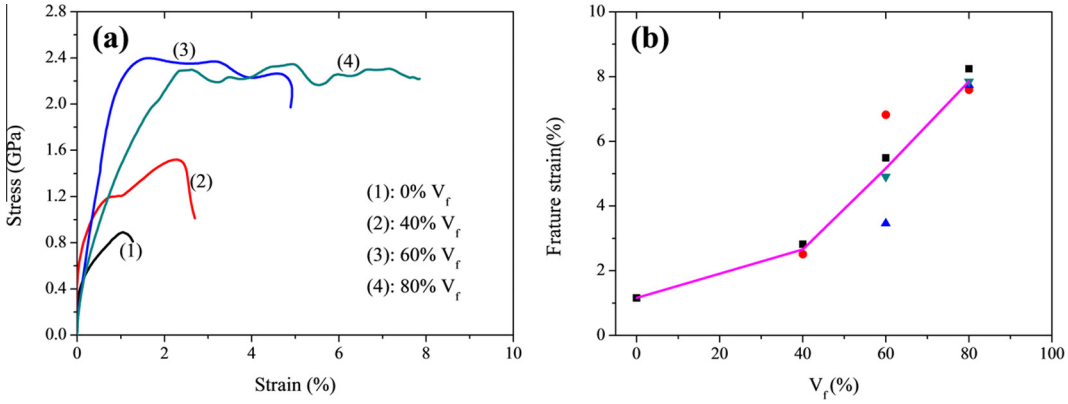

Fig. 11. (a) Stress–strain curves of the composite with different fiber volume fractions under dynamic compression. (b) Fracture strain of the composite varies with the fiber volume fraction V_f under dynamic compression.

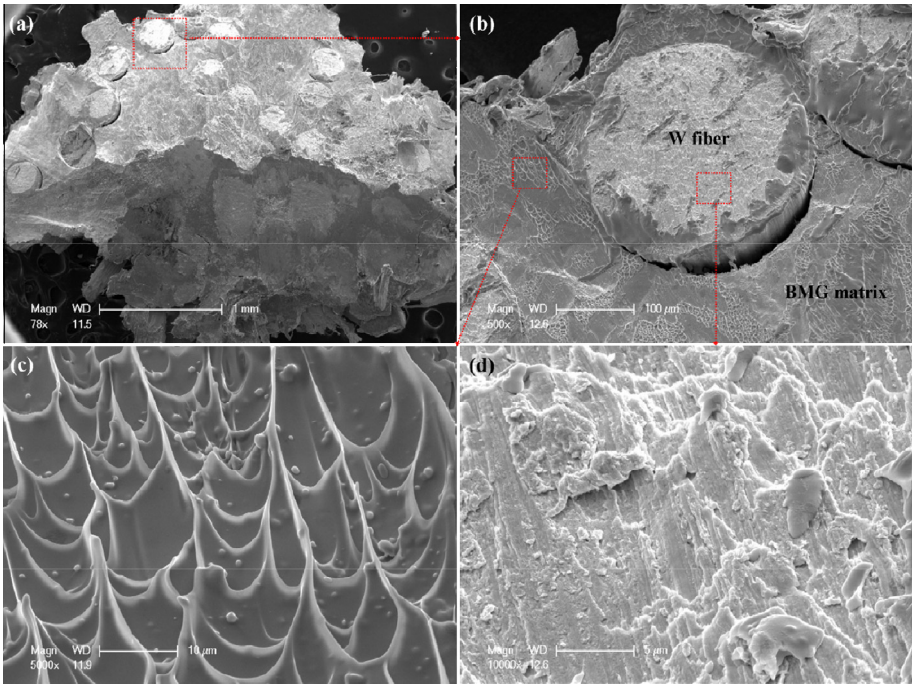

Fig. 12. Fracture morphologies of the 40% V_f under dynamic compression. (a) Top-view of the fractured specimen. (b) Magnified image of the marked area in (b). (c) And (d) show details corresponding to the areas marked in (b).

propagation of the composite increases with the increasing fiber volume fraction, i.e., shear banding becomes more difficult for the composite with high fiber volume fraction. However, with the increasing fiber volume fraction, the critical energy for splitting of the tungsten fiber/Vit 1 composite Γ_{SP} decreases, indicating that the composite with high fiber volume fraction has a weaker resistance to splitting. Γ_{SP} and Γ_{SB} intersect at a critical fiber volume fraction V_c. For $V_f < V_c$, Γ_{SP} is higher than Γ_{SB}. This indicates that splitting fracture needs more energy to be activated. In this case, shear banding would be more active than splitting. Thus, shear banding will dominate the deformation of the composite. For $V_f > V_c$, the energy needed for shear banding overtakes that needed for splitting, indicating splitting would be easier to take place than shear banding. Thus, splitting will become the dominant failure mode of the composite. V_c is the critical fiber volume fraction for shear-split fracture transition.

Under quasi-static compression, the local strain rate can be obtained from the deformation process recorded by the high speed camera and SEM observations, which is on the order of 10^0/s. Under this strain rate, the variation of Γ_{SB} and Γ_{SP} with the fiber volume fraction V_f can be obtained from Eqs. (1)-(3) and (8)-(10), respectively, as plotted in Fig. 16. With the increasing fiber volume fraction V_f, Γ_{SB} increases, while Γ_{SP} decreases. These indicates that the resistance to shear banding of the composite increases but the resistance to splitting decreases with the increasing fiber volume fraction V_f. This is consistent with the experimental results, as shown in Table 1. Γ_{SB} and Γ_{SP} intersect at the 62% V_f. For $V_f < 62\%$, Γ_{SP} is higher than Γ_{SB}. Shear banding would be more active than splitting. This illustrates why the composite with 0% V_f and 40% V_f fails by shear banding under quasi-static compression. For composite with 60% V_f, the energy needed for shear banding and splitting are about the same. In this case, the composite will fracture in a mixed mode, as shown in Fig. 8(a). However, splitting will dominate the fracture finally. For $V_f > 62\%$, Γ_{SP} becomes lower than Γ_{SB}. This indicates that more energy is needed for shear banding than that needed for splitting. Splitting becomes dominant

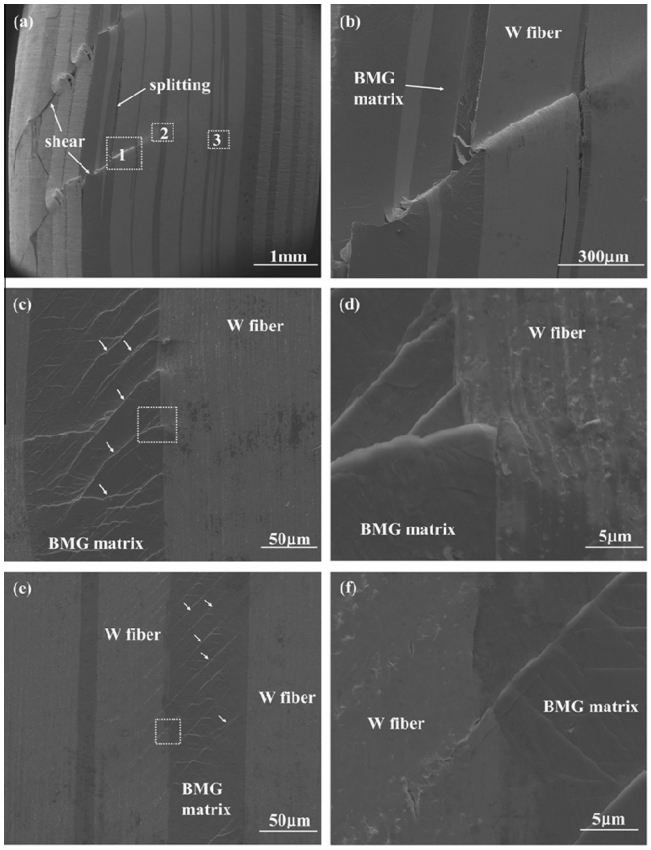

Fig. 13. Fracture morphologies of the 60% V_f under dynamic compression. (a) Lateral surface of fractured specimen. (b), (c) and (e) are magnified images of the areas marked by (1)-(3) in (a), respectively. Multiple shear bands are shown by the arrows. (d) And (f) show details corresponding to the areas marked in (c) and (e), respectively.

failure mode of the composite. Thus, the composite with 80% V_f fails in the splitting mode. The critical fiber volume fraction for shear banding-splitting fracture transition is about 60% under quasi-static strain rate.

For composite under dynamic compression, it is difficult to obtain the exact value of local shear strain rate. However, it can be seen from Fig. 15 that under the high strain rate, there still exist the competition between the shear banding and splitting. Similar to the quasi-static case, for composite with V_f lower than the critical fiber volume fraction V_c, critical energy dissipated within the shear band Γ_{SB} is lower than critical energy for splitting Γ_{SP}, shear banding will occur. For composite with V_f higher than the V_c, Γ_{SB} increases and becomes higher than Γ_{SP}. Composite will fail by splitting fracture in this case. This is consistent with the experimental results observed under dynamic compression.

Another factor to affect the failure behavior of the composite is the strain rate. Under quasi-static loading, composite with 60% V_f failure in splitting dominated mode. However, as the strain rate increases to dynamic case, shear dominated fracture occurs for the 60% V_f composite. With the increasing strain rate, the critical energy dissipated within shear band of the composite will decrease, as shown in Fig. 15. This leads to higher critical fiber volume fraction V_c for shear banding-splitting fracture transition. The V_c varies with the strain rate is shown in Fig. 17. It can be seen from this plot that V_c increases with increasing strain rate. This demonstrates that for the composite with a specific fiber volume fraction V_f, shear banding is more likely to occur under high strain rate. This illustrates the reason for the transition of failure mode from splitting dominated mode in quasi-static strain rate to shear dominated mode under dynamic loading for the 60% V_f composite. Furthermore, from Fig. 17, it can be concluded that 80% V_f composite can failure by shear under the strain rate high enough. This shear banding will lead to "self-sharpening" behavior of the composite under ballistic impact, and penetrator performance can be improved significantly (Conner et al., 2000).

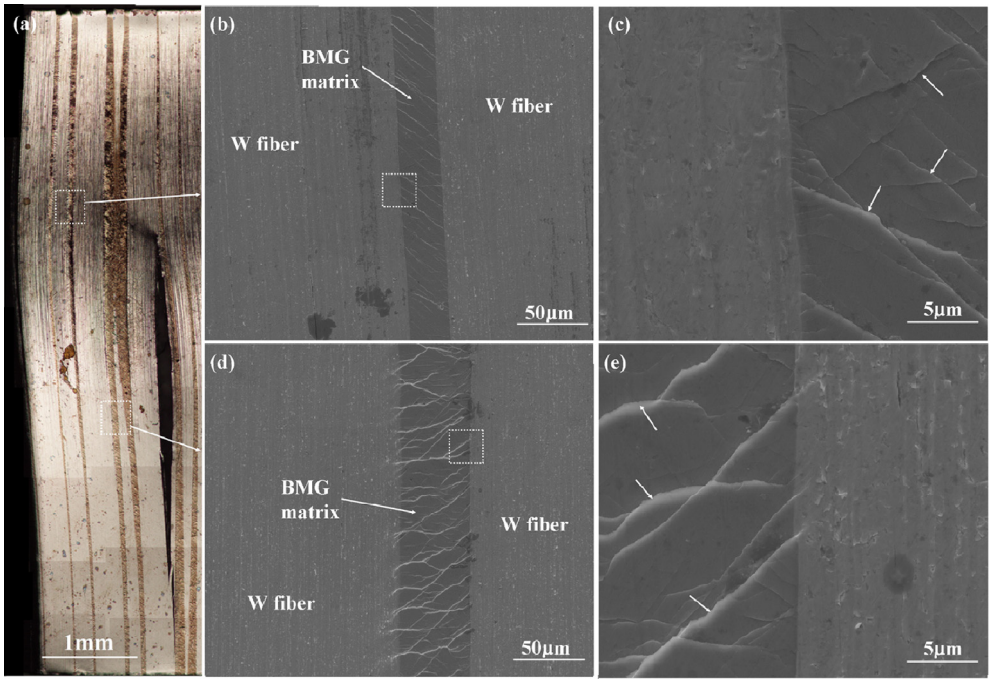

Fig. 14. Fracture morphologies of the 80% V_f under dynamic compression. (a) Lateral surface of fractured specimen under optical microscope. (b) And (d) are magnified images of the areas marked in (a), respectively. (c) And (e) show details corresponding to the areas marked in (c) and (e), respectively. Multiple shear bands are shown by the arrows.

Table 2
Thermodynamic parameters of the tungsten fiber.

ρ (kg/m^3 × 10^3)	c (J/kg K)	α (K × 10^{-4})	χ (m^2/s × 10^{-5})	τ_y (GPa)
19.3	130	7.0[a]	6.51	1.36[b]

[a] From tungsten alloy.
[b] Calculated from longitudinal tensile stress.

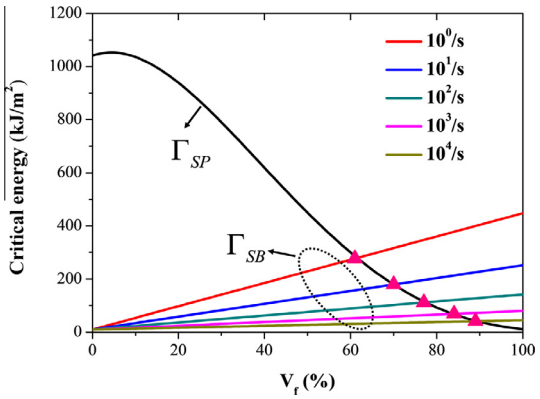

Fig. 15. Critical energy dissipated within shear band of the composite Γ_{SB} and critical energy for splitting of the composite Γ_{SP} vary with the fiber volume fraction V_f under different strain rates.

Table 3
Physical properties of the tungsten fiber and Vit 1 BMG.

	Vit1 BMG	W fiber
Elastic modulus (GPa)	96	410
Poisson's ratio	0.36	0.28
Tensile strength (GPa)	1.8	0.3[a]

[a] Transverse tensile strength.

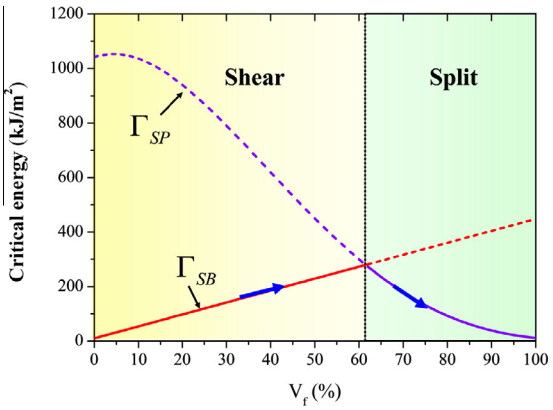

Fig. 16. Competition between Γ_{SB} and Γ_{SP} of the composite under quasi-static compression.

The presented energy competition mechanism may increase our understanding on the compressive failure behavior of the tungsten fiber/Vit 1 BMG composite. From this energy competition mechanism, it can be obtained that with the increasing fiber volume fraction V_f, the deformation dominated by the critical energy dissipated within shear band Γ_{SB} will change to that under the control of the critical energy for splitting Γ_{SP} in the composite, and the failure mode will transform from localized shear to split. The plasticity improves significantly with the increasing V_f. If we want to

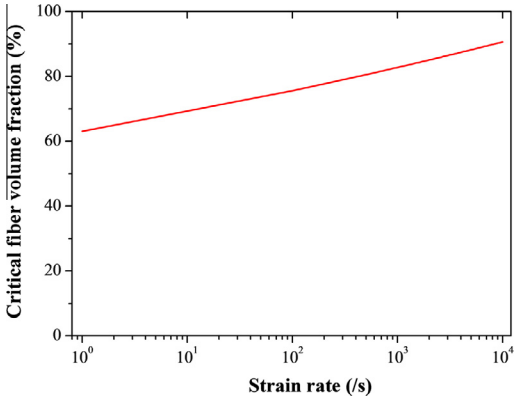

Fig. 17. Critical fiber volume fraction V_c for shear-split transition of the composite varies with strain rate.

get considerable plasticity of this composite under the specific strain rate, the V_f should be higher than the critical fiber volume fraction V_c, which depends on the properties of the tungsten fiber and BMG matrix. However, under high speed impact, we expect that the shear banding occurs for the composite with 80% V_f. This will improve the penetrator performance of the composite. In this case, the impact speed should be high enough to make the critical fiber volume fraction V_c higher than 80%. Otherwise, the 80% V_f composite will fail by splitting and lose its penetrator performance.

The energy competition mechanism can well characterize the compressive failure behavior of the tungsten fiber/Vit 1 composite. However, attention should be paid on the following aspects. (i) During the shear banding, fibrous fracture occurs along (or within) the shear band of tungsten fiber. This is due to the fibrous microstructure along the fiber direction. These new surfaces formation will consume more energy in the shear band, which may increase the critical energy dissipated within the shear band. (ii) In the current model, only elastic deformation energy is considered when calculating the critical energy for splitting, whereas yielding of the composite may occur in the experiments when splitting begins. The yielding of the composite may consume some energy and thus decreases the critical energy for splitting. Actually, in the fiber reinforced polymer composite, non-linear behavior of material was introduced by Steif (1987) and Drapier et al. (1999) to analyze the compressive strength of the composite. It was found by them that the compressive strength is lower than the results based on the elastic analysis which was proposed by Rosen (1964). This suggests that the critical energy for splitting may be reduced by taking the non-linear behavior into account, which deserves a further study in our later work.

5. Conclusions

Transverse tensile, quasi-static and dynamic compressive tests were conducted on the tungsten fiber reinforced $Zr_{41.2}Ti_{13.8}Cu_{10}Ni_{12.5}Be_{22.5}$ bulk metallic glass composite with various fiber volume fractions. The transverse tensile tests show that this composite is a transversely isotropic material. Both the fiber volume fraction and strain rate are found to affect the compressive failure behavior of this composite, which is further characterized by a proposed energy competition mechanism. The competition between the critical energy dissipated within shear band Γ_{SB} and critical energy for splitting Γ_{SP} is found to decide the compressive failure behavior of the composite. Under the specific strain rate, Γ_{SB} dominates the deformation of the composite with low fiber volume fraction V_f, and shear banding occur, while for composite with high fiber volume fraction V_f, Γ_{SP} becomes the dominant factor of the

composite, splitting fracture occurs. Furthermore, the critical fiber volume fraction V_c for shear banding-splitting fracture transition increases with the increasing strain rate, indicating shear banding is more likely to occur for the composite under high strain rate. The proposed energy competition mechanism can well characterize the compressive failure behavior of the tungsten fiber/Vit 1 composite.

Acknowledgments

Financial support is from the National Key Basic Research Program of China (Grant No. 2012CB937500), the NSFC (Grants Nos. 11472287, 11132011, 11202221). Research supported by the CAS/SAFEA International Partnership Program for Creative Research Teams.

Appendix A. Supplementary data

Supplementary data associated with this article can be found, in the online version, at http://dx.doi.org/10.1016/j.ijsolstr.2015.05.008.

References

Argon, A.S., 1979. Plastic deformation in metallic glasses. Acta Metall. 27, 47–58.
Bruck, H.A., Rosakis, A.J., Johnson, W.L., 1996. The dynamic compressive behavior of beryllium bearing bulk metallic glasses. J. Mater. Res. 11, 503–511.
Chen, M.W., 2008. Mechanical behavior of metallic glasses: microscopic understanding of strength and ductility. Annu. Rev. Mater. Res. 39, 445–469.
Chen, J.H., Jiang, M.Q., Chen, Y., Dai, L.H., 2013. Strain rate dependent shear banding behavior of a Zr-based bulk metallic glass composite. Mater. Sci. Eng. A 576, 134–139.
Chen, Y., Jiang, M.Q., Dai, L.H., 2013. Collective evolution dynamics of multiple shear bands in bulk metallic glasses. Int. J. Plast. 50, 18–36.
Chen, J.H., Chen, Y., Jiang, M.Q., Chen, X.W., Fu, H.M., Zhang, H.F., Dai, L.H., 2014. Direct observation on the evolution of shear banding and buckling in tungsten fiber reinforced Zr-based bulk metallic glass composite. Metall. Mater. Trans. A 45 (763–771), 5397–5408.
Conner, R.D., Dandliker, R.B., Johnson, W.L., 1998. Mechanical properties of tungsten and steel fiber reinforced $Zr_{41.25}Ti_{13.75}Cu_{12.5}Ni_{10}Be_{22.5}$ metallic glass matrix composites. Acta Mater. 46, 6089–6102.
Conner, R.D., Dandliker, R.B., Scruggs, V., Johnson, W.L., 2000. Dynamic deformation behavior of tungsten-fiber/metallic-glass matrix composites. Int. J. Impact Eng. 24, 435–444.
Conner, R.D., Li, Y., Nix, W.D., Johnson, W.L., 2004. Shear band spacing under bending of Zr-based metallic glass plates. Acta Mater. 52, 2429–2434.
Dai, L.H., 2012. Shear banding in bulk metallic glasses. In: Dodd, B., Bai, Y.L. (Eds.), Adiabatic Shear Localization: Frontiers and Advances, second ed. Elsevier, London, pp. 311–361.
Dai, L.H., Bai, Y.L., 2008. Basic mechanical behaviors and mechanics of shear banding in BMGs. Int. J. Impact Eng. 35, 704–716.
Dai, L.H., Yan, M., Liu, L.F., Bai, Y.L., 2005. Adiabatic shear banding instability in bulk metallic glasses. Appl. Phys. Lett. 87, 141916.
Dandliker, R.B., Conner, R.D., Johnson, W.L., 1998. Melt infiltration casting of bulk metallic glass matrix composites. J. Mater. Res. 13, 2896–2901.
Das, J., Tang, M.B., Kim, K.B., Theissmann, R., Baier, F., Wang, W.H., Eckert, J., 2005. "Work-hardenable" ductile bulk metallic glass. Phys. Rev. Lett. 94, 205501.
Drapier, S., Grandidier, J.-C., Poitier-Ferry, M., 1999. Towards a numerical model of the compressive strength for long fibre composites. Eur. J. Mech. A 18, 69–92.
Grady, D.E., 1992. Properties of an adiabatic shear band process zone. J. Mech. Phys. Solids 40, 1197–1215.
Grady, D.E., 1994. Dissipation in adiabatic shear bands. Mech. Mater. 17, 289–293.
Greer, A.L., Cheng, Y.Q., Ma, E., 2013. Shear bands in metallic glasses. Mater. Sci. Eng. R 74, 71–132.
Gu, X.J., Poon, S.J., Shiflet, G.J., Widom, M., 2008. Ductility improvement of amorphous steel: role of shear modulus and electronic structure. Acta Mater. 56, 88–94.
Gu, X.J., Poon, S.J., Shiflet, G.J., Lewandowski, J.J., 2010. Compressive plasticity and toughness of a Ti-based bulk metallic glass. Acta Mater. 58, 1708–1720.
Hays, C.C., Kim, C.P., Johnson, W.L., 2000. Microstructure controlled shear band pattern formation and enhanced plasticity of bulk metallic glasses containing in situ formed ductile phase dendrite dispersions. Phys. Rev. Lett. 84, 2901–2904.
Hofmann, D.C., Suh, J.-Y., Wiest, A., Duan, G., Lind, M.-L., Demetriou, M.D., Johnson, W.L., 2008a. Designing metallic glass matrix composites with high toughness and tensile ductility. Nature 451, 1085–1089.
Hofmann, D.C., Suh, J.-Y., Wiest, A., Lind, M.-L., Demetriou, M.D., Johnson, W.L., 2008b. Development of tough, low-density titanium-based bulk metallic glass matrix composites with tensile ductility. PNAS 105, 20136–20140.
Hou, B., Li, Y.-L., Xing, L.-Q., Chen, C.-S., Kou, H.-C., Li, J.-S., 2007. Dynamic and quasi-static mechanical properties of fiber-reinforced metallic glass at different temperatures. Philos. Mag. Lett. 87, 595–601.
Jiang, M.Q., Dai, L.H., 2009. On the origin of shear banding instability in metallic glasses. J. Mech. Phys. Solids 57, 1267–1292.
Jiang, M.Q., Dai, L.H., 2011. Shear band toughness of bulk metallic glasses. Acta Mater. 59, 4525–4537.
Jiang, W.H., Fan, G.J., Liu, F.X., Wang, G.Y., Choo, H., Liaw, P.K., 2008a. Spatiotemporally inhomogeneous plastic flow of a bulk metallic glass. Int. J. Plast. 24, 1–16.
Jiang, M.Q., Ling, Z., Meng, J.X., Dai, L.H., 2008b. Energy dissipation in fracture of bulk metallic glass via inherent competition between local softening and quasi-cleavage. Philos. Mag. 88, 407–426.
Leber, S., Tavernelli, J., White, D.D., 1976. Fracture modes in tungsten wire. J. Less Common Met. 48, 119–133.
Lee, S.-B., Lee, S.-K., Lee, S.H., Kim, N.J., 2008. Microstructure and mechanical properties of two continuous-fiber-reinforced Zr-based amorphous alloy composites fabricated by liquid pressing process. Metall. Mater. Trans. A 39, 763–771.
Lewandowski, J.J., 2001. Effects of annealing and changes in stress state on fracture toughness of bulk metallic glass. Mater. Trans. 42, 633–637.
Lewandowski, J.J., Greer, A.L., 2006. Temperature rise at shear bands in metallic glasses. Nat. Mater. 5, 15–18.
Lewandowski, J.J., Wang, W.H., Greer, A.L., 2005. Intrinsic plasticity or brittleness of metallic glass. Philos. Mag. Lett. 85, 77–87.
Li, H., Subhash, G., Gao, X.-L., Kecskes, L.J., Dowding, R.J., 2003. Negative strain rate sensitivity and compositional dependence of fracture strength in Zr/Hf based bulk metallic glasses. Scr. Mater. 49, 1087–1092.
Liu, L.F., Dai, L.H., Bai, Y.L., Wei, B.C., Eckert, J., 2005a. Behavior of multiple shear bands in Zr-based bulk metallic glass. Mater. Chem. Phys. 93, 174–177.
Liu, L.F., Dai, L.H., Bai, Y.L., Wei, B.C., 2005b. Initiation and propagation of shear bands in Zr-based bulk metallic glass under quasi-static and dynamic shear loadings. J. Non Cryst. Solids 351, 3259–3270.
Liu, Y.H., Wang, G., Wang, R.J., Zhao, D.Q., Pan, M.X., Wang, W.H., 2007. Super plastic bulk metallic glasses at room temperature. Science 315, 1385–1388.
Ma, W.F., Kou, H.C., Chen, C.S., Li, J.S., Chang, H., Zhou, L., Fu, H.Z., 2008. Compressive deformation bahaviors of tungsten fiber reinforced Zr-based metallic glass composites. Mater. Sci. Eng. A 486, 308–312.
Martin, M., Kecskes, L., Thadhani, N.N., 2008. Dynamic compression of a zirconium-based metallic glass confined by a stainless steel sleeve. Scr. Mater. 59, 688–691.
Martin, M., Meyer, L., Kecskes, L., Thadhani, N.N., 2009. Uniaxial and biaxial compressive response of a bulk metallic glass composite over a range of strain rates and temperatures. J. Mater. Res. 2009, 66–78.
Meyers, M.A., Nesterenko, V.F., LaSalvia, J.C., Xue, Q., 2001. Shear localization in dynamic deformation of materials: microstructural evolution and self-organization. Mater. Sci. Eng. A 317, 204–225.
Qiao, J.W., Sun, A.C., Huang, E.W., Zhang, Y., Liaw, P.K., Chuang, C.P., 2011. Tensile deformation micromechanisms for bulk metallic glass matrix composites: from work-hardening to softening. Acta Mater. 59, 4126–4137.
Qiu, K.Q., Wang, A.M., Zhang, H.F., Ding, B.Z., Hu, Z.Q., 2002. Mechanical properties of tungsten fiber reinforced ZrAlNiCuSi metallic glass matrix composite. Intermetallics 10, 1283–1288.
Rosen, B.W., 1964. Mechanisms of Composite Strengthening. In: Fiber Composite Materials. American Society of Metals, Cleveland, OH, pp. 37–75 (Chapter 3).
Ruan, H.H., Zhang, L.C., Lu, J., 2011. A new constitutive for shear banding instability in metallic glass. Int. J. Solids Struct. 48, 3112–3127.
Son, C.-Y., Kim, G.S., Lee, S.-B., Lee, S.-K., Kim, H.S., Lee, S.H., 2012. Dynamic compressive properties of Zr-based amorphous matrix composites reinforced with tungsten continuous fibers or porous foams. Metall. Mater. Trans. A 43, 1911–1920.
Spaepen, F., 1977. A microscopic mechanism for steady state inhomogeneous flow in metallic glass. Acta Metall. 25, 407–415.
Steif, P.S., 1987. An exact two-dimensional approach to fiber micro-buckling. Int. J. Solids Struct. 23, 1235–1246.
Subhash, G., Dowding, R.J., Kecskes, L.J., 2002. Characterization of uniaxial compressive of bulk amorphous Zr–Ti–Cu–Ni–Be alloy. Mater. Sci. Eng. A 334, 33–40.
Sunny, G., Lewandowski, J., Prakash, V., 2007. Effects of annealing and specimen geometry on dynamic compression of a Zr-based bulk metallic glass. J. Mater. Res. 22, 389–401.
Sunny, G., Yuan, F.P., Prakash, V., Lewandowski, J.J., 2008. Effect of high strain rates on peak stress in a Zr-based bulk metallic glass. J. Appl. Phys. 104, 093522.
Sunny, G., Yuan, F., Prakash, V., Lewandowski, J., 2009. Design of inserts for split-Hopkinson pressure bar testing of low strain-to-failure materials. Exp. Mech. 49, 479–490.
Trexler, M.M., Thadhani, N.N., 2010. Mechanical properties of bulk metallic glasses. Prog. Mater. Sci. 55, 759–839.
Varge, L., Bartha, L., Nagy, A.J., Stefaniay, V., Borossary, B., 1974. Proceedings of the Fifth Conference on Dimensioning and Strength Calculations, vol. 1. Akademiai Kiado, Budapest, p. 236.
Wang, W.H., 2012. The elastic properties, elastic models and elastic perspectives of metallic glasses. Prog. Mater. Sci. 57, 487–656.
Wang, G., Chen, D.M., Shen, J., Stachurski, Z.H., Qin, Q.H., Sun, J.F., Zhou, B.D., 2006. Deformation behaviors of a tungsten-wire/bulk metallic glass matrix composite in a wide strain rate stage. J. Non Cryst. Solids 352, 3872–3878.
Wang, H., Zhang, H.F., Hu, Z.Q., 2007. Tungsten fiber reinforced Zr-based bulk metallic glass composites. Mater. Manuf. Process. 22, 687–691.

Wang, G.Y., Liaw, P.K., Morrison, M.L., 2009. Progress in studying the fatigue behavior of Zr-based bulk metallic glasses and their composites. Intermetallics 17, 579–590.

Wu, Y., Xiao, Y.H., Chen, G.L., Liu, C.T., Lu, Z.P., 2010. Bulk metallic glass composites with transformation mediated work-hardening ductility. Adv. Mater. 22, 2770–2773.

Wu, Y., Wang, H., Wu, H.H., Zhang, Z.Y., Hui, X.D., Chen, G.L., Ma, D., Wang, X.L., Lu, Z.P., 2011. Formation of Cu–Zr–Al bulk metallic glass composites with improved tensile properties. Acta Mater. 59, 2928–2936.

Xu, J., Ma, E., 2014. Damage-tolerant Zr–Cu–Al-based bulk metallic glasses with record-breaking fracture toughness. J. Mater. Res. 29, 1489–1499.

Yang, B., Morrison, M.L., Liaw, P.K., Buchanan, R.A., Wang, G.Y., Liu, C.T., Denda, M., 2005. Dynamic evolution of nanoscale shear bands in a bulk metallic glass. Appl. Phys. Lett. 86, 141904.

Yang, B., Liu, C.T., Nieh, T.G., Morrsion, M.L., Liaw, P.K., Buchanan, R.A., 2006. J. Mater. Res. 21, 915–922.

Yang, Y., Ye, J.C., Lu, J., Liaw, P.K., Liu, C.T., 2010. Characteristic length scales governing plasticity/brittleness of bulk metallic glasses at ambient temperature. Appl. Phys. Lett. 96, 011905.

Yao, K.F., Ruan, F., Yang, Y.Q., Chen, N., 2006. Superductile bulk metallic glass. Appl. Phys. Lett. 88, 122106.

Yim, H.C., Busch, R., Koster, U., Johnson, W.L., 1999. Synthesis and characterization of particulate reinforced $Zr_{57}Nb_5Al_{10}Cu_{15.4}Ni_{12.6}$ bulk metallic glass composites. Acta Mater. 47, 2455–2462.

Yuan, F.P., Prakash, V., Lewandowski, J.J., 2007. Spall strength and Hugoniot elastic limit of Zirconium-based bulk metallic glass under planar shock compression. J. Mater. Res. 22, 402–411.

Yuan, F.P., Prakash, V., Lewandowski, J.J., 2009. Spall strength of a zirconium-based bulk metallic glasses under shock-induced compression and shear loading. Mech. Mater. 41, 886–897.

Zhang, H., Zhang, Z.F., Wang, Z.G., Qiu, K.Q., Zhang, H.F., Zang, Q.S., 2006. Effects of tungsten fiber on failure mode of Zr-based bulk metallic glassy composite. Metall. Mater. Trans. A 37, 2459–2469.

Zhang, H., Zhang, Z.F., Wang, Z.G., Zhang, H.F., 2008. Deformation and damage evolution of tungsten fiber reinforced metallic glass matrix composite induce by compression. Mater. Sci. Eng. A 483–484, 164–167.

Zhang, H.W., Maiti, S., Subhash, G., 2008. Evolution of shear bands in bulk metallic glasses under dynamic loading. J. Mech. Phys. Solids 56, 2171–2187.

Zhang, H.F., Li, H., Wang, A.M., Fu, H.M., Ding, B.Z., Hu, Z.Q., 2009. Synthesis and characteristics of 80 vol.% tungsten (W) fibre/Zr based metallic glass composite. Intermetallics 17, 1070–1077.